



Accepted Article

Title: Ultrafine CuO Particles Dispersed on Nitrogen-Doped Carbon Hollow Nanospheres for Oxidative Esterification of Biomass-Derived 5-Hydroxymethylfurfural

Authors: Shyam Sunder R. Gupta, Ajayan Vinu, and Lakshmikantam Mannepalli

This manuscript has been accepted after peer review and appears as an Accepted Article online prior to editing, proofing, and formal publication of the final Version of Record (VoR). This work is currently citable by using the Digital Object Identifier (DOI) given below. The VoR will be published online in Early View as soon as possible and may be different to this Accepted Article as a result of editing. Readers should obtain the VoR from the journal website shown below when it is published to ensure accuracy of information. The authors are responsible for the content of this Accepted Article.

To be cited as: *ChemPlusChem* 10.1002/cplu.202000713

Link to VoR: <https://doi.org/10.1002/cplu.202000713>

Accepted Article

Ultrafine CuO Particles Dispersed on Nitrogen-Doped Carbon Hollow Nanospheres for Oxidative Esterification of Biomass-Derived 5-Hydroxymethylfurfural

Shyam Sunder R. Gupta[†], Prof. Ajayan Vinu[‡] and Prof. Mannepalli Lakshmi Kantam^{†,*}

[†] *Department of Chemical Engineering, Institute of Chemical Technology, Matunga (E), Mumbai - 400019, Maharashtra, India.*

[‡] *Global Innovative Center for Advanced Nanomaterials (GICAN), School of Engineering, Faculty of Engineering and Built Environment, The University of Newcastle, Callaghan, NSW 2308, Australia.*

Corresponding author E-mail: lk.mannepalli@ictmumbai.edu.in

Abstract: One-pot synthesis of furan-2,5-dimethylcarboxylate (FDMC) from 5-hydroxymethylfurfural (HMF) is highly demanding for the commercial production of polyethylene furanoate (PEF). Herein, we report a direct synthesis of FDMC from oxidative esterification of HMF using ultrafine CuO particles dispersed on nitrogen-doped carbon hollow nanospheres (CuO/N-C-HNSs) as a catalyst and *tert*-butyl hydroperoxide (TBHP) as an oxidizing and methylating reagent. The CuO/N-C-HNSs was prepared through a template protection-sacrifice strategy using SiO₂ as a sacrificial template and histidine as the precursor for N and C. N-doping facilitated a strong interaction between the support and copper species, affording formation of CuO nanoparticles of less than 10 nm in size. By virtue of the highly dispersed CuO nanoparticles and a high BET surface area 373 m²/g, the CuO/N-C-HNSs shows excellent catalytic performance in selective conversion of HMF into FDMC affording 93% yield of the desired product with a TON value of 49. Furthermore, the oxidative esterification involving *SP*³ C-H bond functionalization is also demonstrated using the same catalyst.

Keywords: heterogeneous catalysis; 5-hydroxymethylfurfural; nanostructures; N-doped carbon; oxidative esterification

1. Introduction

Utilization of carbon-neutral biomass as a renewable resource for the production of fuels and value-added chemicals is a promising approach to overcome the rapid consumption of fossil resources and environmental deterioration due to the emission of CO₂.^[1-7] Among a broad

spectrum of biomass-derived molecules, 5-hydroxymethylfurfural (HMF) obtained from acid-catalyzed hydrolysis of cellulose, has attracted the significant attention of researchers due to its versatile applications in fuel^[8] pharmaceutical^[9] and polymer^[10] industries. Selective oxidation of HMF affords 2,5-furandicarboxylic acid^[11–16] (FDCA) which is an important raw material used for the synthesis of polyethylene furanoate (PEF), a bio-based renewable polymer, through a simple polymerization with ethylene glycol.^[17] PEF is identified as a suitable replacement for the petroleum-derived polyethylene terephthalate (PET)^[18]. As compared to PET, PEF exhibits superior material properties including high tensile strength, high glass transition temperature, high isolation rate of CO₂, O₂ and water and easy enzymatic hydrolysis.^[19,20] Despite the significant progress that has been made in the production of FDCA, a direct polymerization of FDCA with ethylene glycol is less preferred because the quantitative isolation of FDMC in high purity for polymerization is challenging.^[21] The high boiling point and poor solubility of FDCA in numerous solvents make its purification difficult by distillation and recrystallization techniques.^[22] Furthermore, the undesirable side reactions, including decarboxylation of FDCA during polymerization, produces a low quality PEF.^[23] These issues may be overcome by converting FDCA into furan-2,5-dimethylcarboxylate (FDMC) through esterification. In contrast to FDCA, FDMC is soluble in various industrial solvents and possesses a low boiling point. In addition, it can be purified by a low temperature sublimation process and can be used directly for the polymerization with ethylene glycol to obtain a high quality PEF.^[17,24] Therefore, a simple and one-pot conversion of HMF into FDMC is in high demand since such processes will improve the quality as well as cost in commercial production of PEF (Fig. 1).

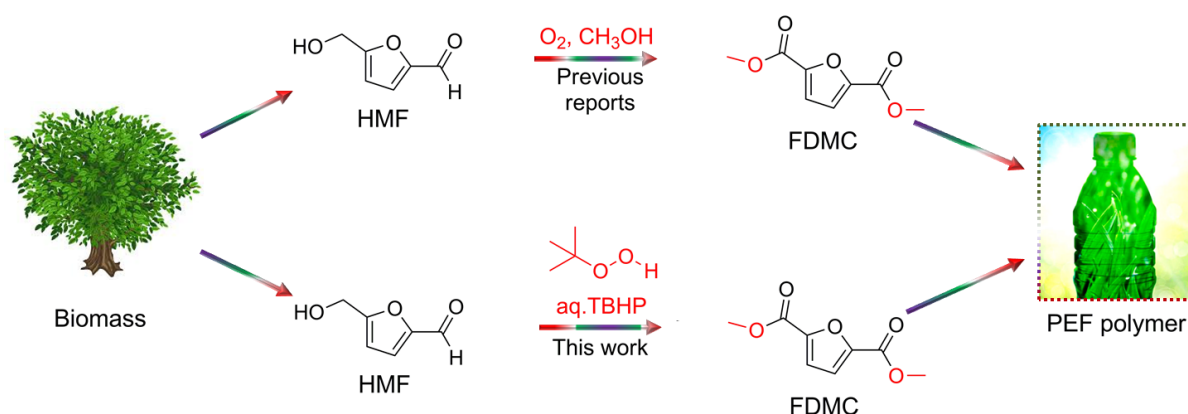


Fig. 1 Previous and the current approaches used for synthesis of FDMC from HMF.

Considering these benefits, several researchers are continuously working for the development of highly efficient catalytic systems for one-pot conversion of HMF into FDMC. In this

regard, Christensen and co-workers reported the pioneering work on one-pot conversion of HMF into FDMC in presence of molecular oxygen and sodium methoxide using Au/TiO₂ as a catalyst.^[25] Subsequently, Corma and co-workers reported the aerobic oxidative esterification of HMF using gold supported nano-ceria catalyst in absence of any base and concluded that the Lewis acidity associated with cerium helps in the oxidation of alcohol group present in HMF.^[26] Inspired by the excellent catalytic activity of gold, several other catalyst containing gold as the active metal were designed and explored for the one-pot conversion of HMF into FDMC.^[27–32] Considering the limited availability, and a high cost of gold, precious metal-free oxidative esterification of HMF was also investigated by several researchers. In this regard, Fu and co-workers prepared a pyrolyzed Co_xO_y-N@C material which exhibited an excellent catalytic performance when applied in combination with a co-catalyst K-OMS-2 in aerobic oxidative esterification of HMF and provided 96% yield the desired product.^[33] Xu and co-workers studied the catalytic activity of CoO_x-N/C in combination with α-MnO₂ towards base free synthesis of FDMC from HMF and proposed that the pyridinic nitrogen present in the catalyst acts as a base and facilitates the oxidation of the alcoholic functional group present in HMF.^[34] Recently Cai and co-workers prepared a Zeolitic Imidazole Framework-derived hollow Co@CN material via a template protection-sacrifice (TPS) method using SiO₂ as a sacrificial template and evaluated its catalytic performance in base free one-pot conversion of HMF into FDMC. They concluded that the hollow structure obtained from the removal of SiO₂ facilitates the mass transfer of reactants and products during the reaction thereby regenerating the catalytically active sites.^[35] Inspired by the excellent performance of cobalt, a wide variety of materials containing cobalt were designed and fabricated for one-pot conversion of HMF into FDMC.^[36–43] The above-mentioned processes are highly efficient and provides excellent yield of FDMC from oxidative esterification of HMF using air or molecular oxygen as an economical and readily available oxidizing agent. However, from academic research point of view, the exploration of alternate methods for the synthesis of FDMC from HMF using different oxidizing agents is also important.

Herein, we demonstrate an alternate and unique strategy for the oxidative-methyl esterification of HMF into FDMC using *tert*-butyl hydroperoxide (TBHP) as an oxidant and methylating reagent catalyzed by a novel nanocomposite, CuO/N-C-HNSs (ultrafine CuO particles dispersed on Nitrogen-doped carbon hollow nanospheres). The use of TBHP for methyl-esterification of various oxygenates such as benzyl alcohols, benzaldehydes and benzoic acids was explored by Ghosh et al. using Pd/Cu₂Cl(OH)₃ as a catalyst and K₂CO₃ as

a base additive.^[44] Recently, we have explored a base free synthesis of FDMC via oxidative methyl-esterification of HMF in presence of TBHP using mesoporous alumina nanospheres-embedded with CuO nanoparticles as a catalyst.^[45] In present work, we have fabricated a novel nanomaterial, CuO/N-C-HNSs for the oxidative esterification reaction. The hollow spherical structure induces a high mesoporosity which facilitates the mass transfer of reactants as well as products during the reaction. N-doped carbon materials provide ultra-high dispersion of metals in the form of fine particles or even as single atoms.^[46,47] N-doping firmly stabilizes the metal nanoparticles through a strong interaction between the metal and the support and mitigates their aggregation during the reaction.^[48] Considering these advantages, N-C-HNSs with ultrafine dispersion of CuO particles was prepared by a template protection-sacrifice strategy using SiO₂ as a hard template and histidine as the precursor for N and C.^[49] The overall synthesis of CuO/N-C-HNSs is schematically illustrated in Figure 2. At-first, SiO₂ nanospheres having particle sizes in the range of 100-150 nm were prepared by a modified Stöber's method.^[50] Next, the surface of the as-prepared SiO₂ nanospheres was modified with negative charges using NaCl, PDDA and PSS polymers. Once the SiO₂ nanospheres are modified with the negative charges, Cu²⁺ ions gets strongly adsorbed on their surface through electrostatic force of attraction. Subsequently, the histidine molecule containing an amine, a carboxylic acid and an imidazole group binds with the Cu²⁺ ions through coordination interaction and results in to the formation of SiO₂@His-Cu nanospheres. Finally, the high-temperature pyrolysis followed by silica etching afforded highly dispersed CuO nanoparticles on the surface of N-C-HNSs. In addition to HMF, a wide variety of substrates were also converted in to the corresponding esters through functionalization of a less reactive *SP*³ C-H bond (Table 2). Thus the present synthetic methodology can also be used for the synthesis various organic compounds. TBHP has been utilized as an multitasking reagent in several organic reactions^[44,51-56] and here also it acts as an oxidizing and methylating reagent. Furthermore, the pyridinic N present in CuO/N-C-HNSs eliminates the use of an external base.

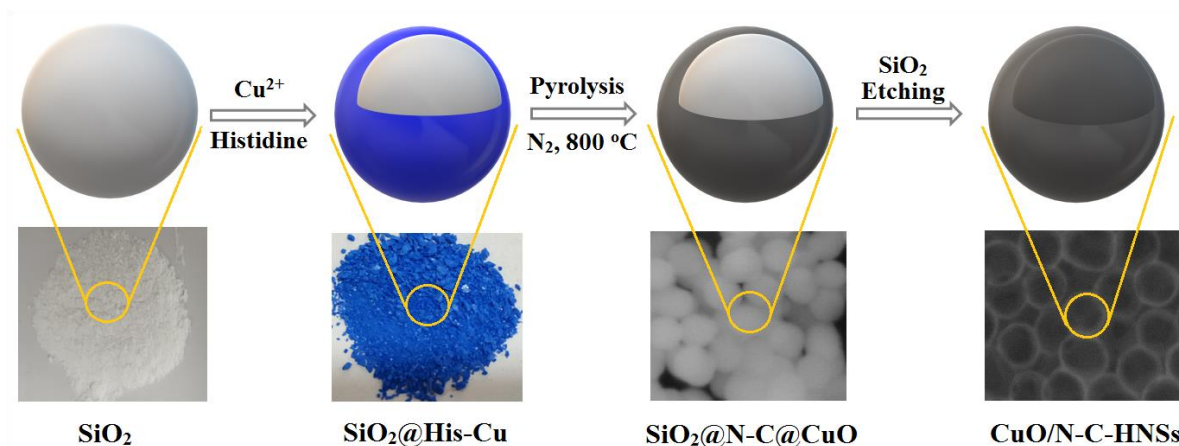


Fig. 2 Schematic representation of the CuO/N-C-HNSs synthesis.

2. Results and discussion

2.1 Catalyst characterization

Field emission gun-scanning electron microscopy (FEG-SEM) images (Fig. 3a and b) and transmission electron microscopy (TEM) image (Fig. 4a) show the formation of spherical shaped SiO₂ nanoparticles having a diameters between 100-150 nm. The formed SiO₂ nanospheres were used as the sacrificial template for the synthesis of CuO/N-C-HNSs. The as-fabricated CuO/N-C-HNSs after removal of SiO₂ by etching remained intact as hollow nanospheres and retained the original size and morphology of the SiO₂ nanoparticles (Fig. 3c and d). The high surface area and mesoporosity resulting from these hollow nanostructures facilitate the effective mass transfer of reactants and products during the oxidative methylesterification process. The well-defined hollow morphology of the CuO/N-C-HNSs was further verified by TEM (Fig. 4b and c). The high-resolution transmission electron microscope (HRTEM) image reveals the presence of ultrafine CuO particles of 5-10 nm in size on the surface of N-C-HNSs (Fig. 4d). The measured interplanar spacing of the nanoparticle is around 0.25 nm (Fig. 4d) corresponding to the CuO (-111) plane. The concentric rings in the selected area electron diffraction (SAED) pattern (Fig. 4f) reveal the polycrystalline nature of the CuO nanoparticles. The presence of ultrafine CuO particles on N-C-HNSs was further verified by electron energy loss spectroscopy (EELS) coupled high-angle annular dark-field scanning transmission electron microscope (HAADF-STEM) imaging. A number of highly dispersed bright dots are observed which correspond to the ultrafine CuO particles (Fig. 4g). Moreover, the EELS elemental mapping shows uniform dispersion of copper on the surface of N-C-HNSs.

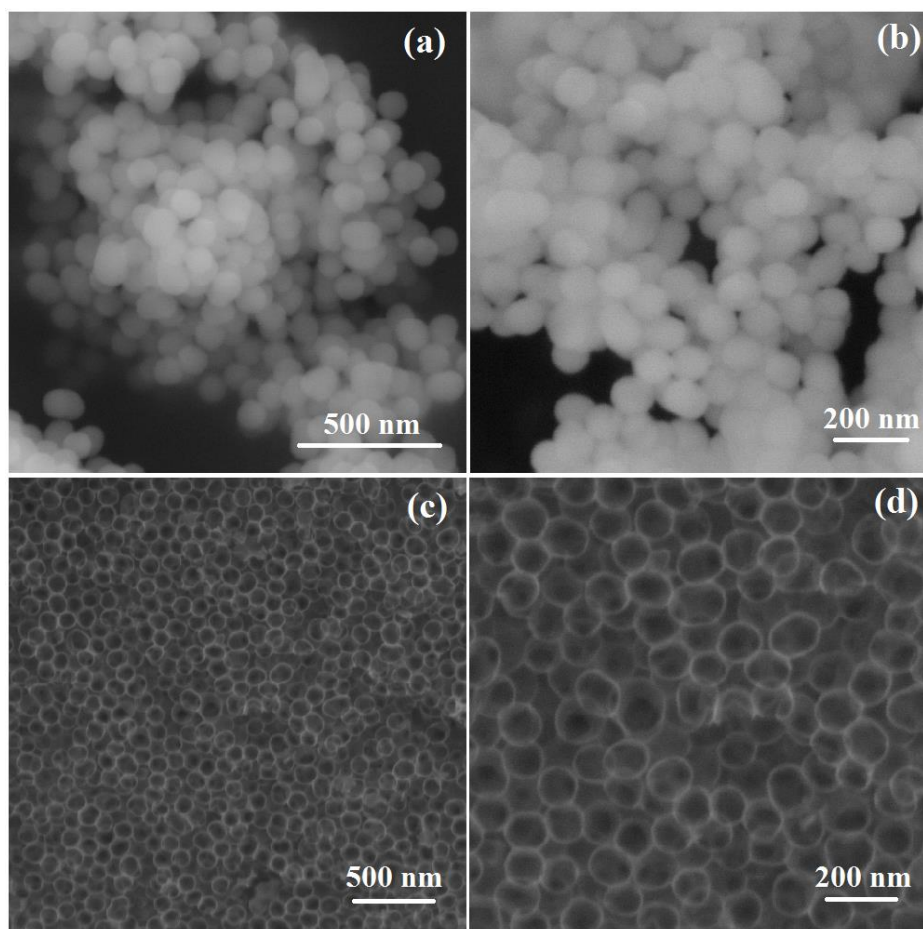


Fig. 3 FEG-SEM images of SiO₂ nanospheres (a) & (b) and CuO/N-C-HNSs (c) & (d).

Phase identification and crystallinity of the as-fabricated materials were examined by recording their powder X-ray diffraction (XRD) patterns (Fig. 5). The as-prepared SiO₂ nanospheres exhibit a broad XRD peak at 22° indicating their amorphous nature.^[57] The XRD peak corresponding to SiO₂ disappeared in CuO/N-C-HNSs after the removal of the template while two new broad peaks appeared at 25° and 44° which can be indexed to (002) and (100) crystal planes of graphitic carbon respectively.^[49,58] The absence of CuO related XRD peaks in CuO/N-C-HNSs could be possibly due to the weak degree of crystallinity of CuO nanoparticles.

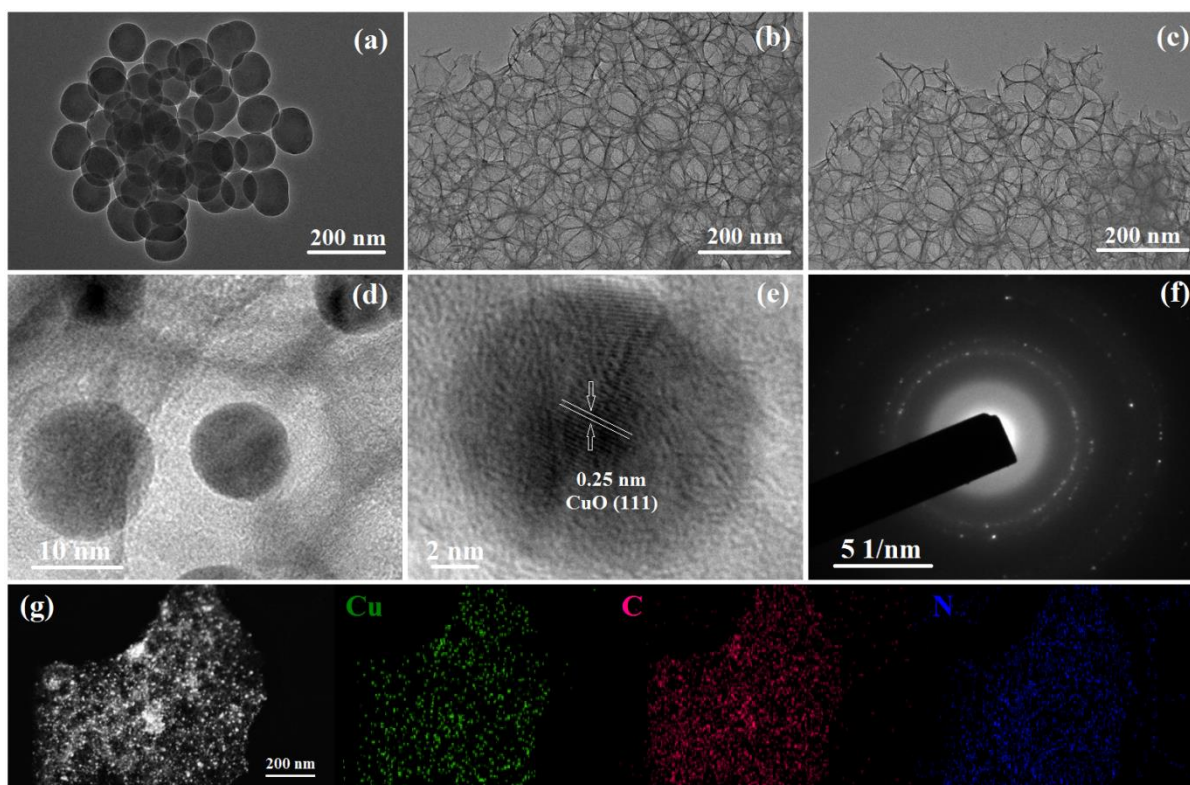


Fig. 4 TEM image of SiO₂ nanospheres (a). TEM images (b) and (c), HRTEM images (d) and (e) and SAED pattern (f) of CuO/N-C-HNSs. HAADF-STEM image and EELS elemental mapping of CuO/N-C-HNSs.

X-ray photoelectron spectroscopy (XPS) analysis was performed to probe the elemental compositions and their chemical states in CuO/N-C-HNSs. The survey scan (Fig. 6a) shows the coexistence of Cu, N, C and O elements in the as-fabricated CuO/N-C-HNSs. The two peaks at 934.7 eV (Cu 2p_{3/2}) and 954.9 eV (Cu 2p_{1/2}) in high-resolution Cu 2p spectrum (Fig. 6b) indicate the presence of CuO.^[59] Additionally, the satellite signals originating at 943.8 eV, and 962.6 eV further confirmed the +2 oxidation state of copper. High-resolution N 1s spectrum (Fig. 6c) reveals the presence of pyridinic N (398.2 eV), graphitic N (399.7 eV) and oxidized form of N (402.4 eV) in CuO/N-C-HNSs.^[48,49] These diverse nitrogen species interact strongly with the copper atoms and stabilize them in the form of ultrafine CuO particles on the surface of N-C-HNSs and also prevents their aggregation during the reaction. The deconvoluted high-resolution C 1s spectrum (Fig. 6d) exhibits three peaks at 284.5 eV, 285.8 eV and 288.8 eV which can be assigned to C-C, C-N and C=O group respectively.^[49] The presence of hysteresis loop in nitrogen adsorption-desorption isotherms (Fig. S2a, ESI) indicates the existence of mesopores in CuO/N-C-HNSs. The pore size distribution curve (Fig. S2b, ESI) reveals that the average diameter of the pores is 4.2 nm. Due to the

mesoporous structure the material possess a large Brunauer-Emmett-Teller (BET) surface area of $373 \text{ m}^2/\text{g}$. Inductively coupled plasma optical emission spectroscopy (ICP-OES) analysis reveals the 2.4 wt% loading of copper in CuO/N-C-HNSs. Thermogravimetric analysis (TGA) analysis (Fig. S1, ESI) exhibits a total of 14 % loss in the weight of CuO/N-C-HNSs when the material was heated up to $800 \text{ }^\circ\text{C}$. The weight loss is predominantly due to evaporation of the trapped moisture from the pores of CuO/N-C-HNSs. The presence of copper in CuO/N-C-HNSs was further verified by recording the XRF spectrum. The XRF spectrum of CuO/N-C-HNSs (Figure S3, ESI) contains a high-intensity peak at 8.05 KeV corresponding to Cu- K_α and a low-intensity peak at 8.93 KeV corresponding to Cu- K_β . Thus, the various characterization results confirm the successful formation of the ultrafine CuO particles dispersed on the surface of N-C-HNSs.

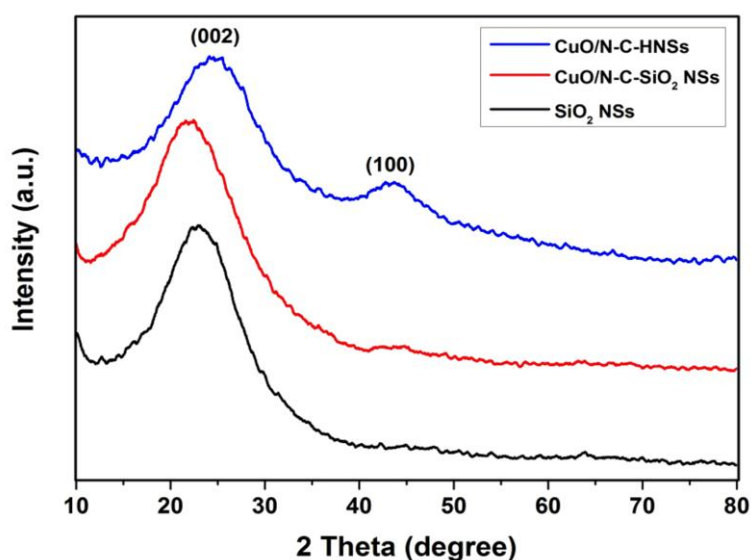


Fig. 5 Powder XRD patterns of the pure silica nanospheres and the CuO functionalized materials.

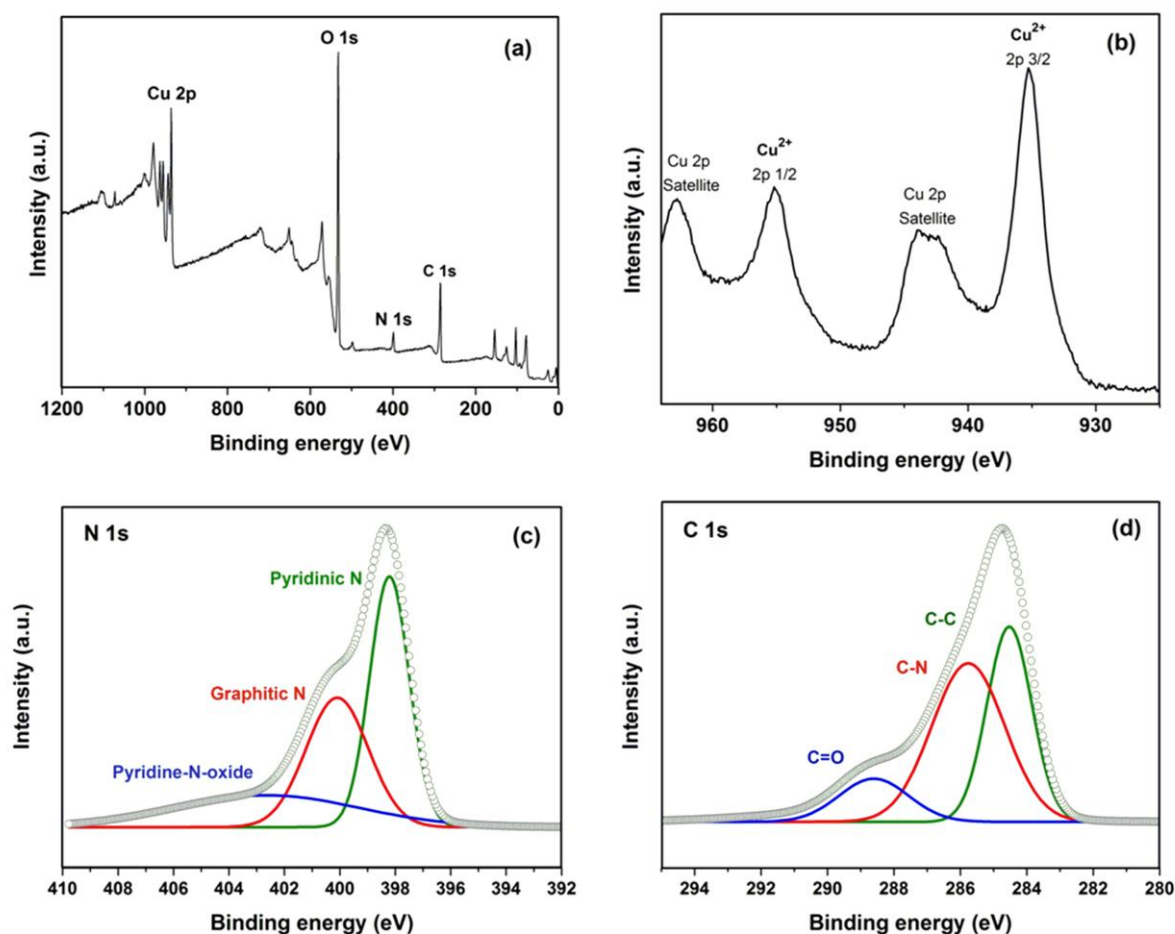


Fig. 6 XPS of CuO/N-C-HNSs (a) survey spectrum, (b) Cu 2p, (c) N 1s and (d) C 1s high-resolution spectrum.

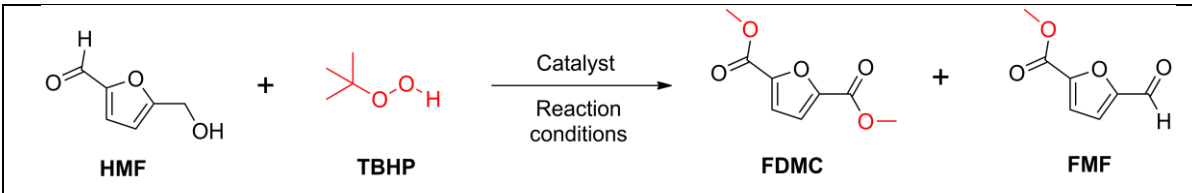
2.2 Catalytic activity

2.2.1 One-pot synthesis of FDMC from HMF

Catalytic activity of the as-fabricated CuO/N-C-HNSs was examined towards one-pot conversion of HMF into FDMC and the results are framed in Table 1. Initially, the reaction was carried out using CuO/N-C-HNSs as the catalyst at 80 °C and 34% of the desired product FDMC was obtained with 66% conversion of HMF (Table 1, entry 1). Next, when temperature of the reaction was increased from 80 °C to 100 °C, the yield of FDMC was also increased from 34% to 93% (Table 1, entries 1-3). However, further increasing the reaction temperature to 110 °C did not improve the yield of FDMC (Table 1, entry 4). Therefore, optimization of the other reaction parameters was carried out at 100 °C. It was noted that, when Nitrogen-doped carbon hollow nanospheres (N-C-HNSs) without any CuO nanoparticles was used as the catalyst, there was no formation of the desired product FDMC

(Table 1, entry 5). This clearly indicates that the catalytic activity of CuO/N-C-HNSs is completely due to the CuO nanoparticles present on the surface of N-C-HNSs. Next, when the reaction was carried out using bulk CuO nanopowder (particle sizes below 50 nm) as the catalyst, 56% yield of FDMC was obtained with a poor TON of 1 (Table 1, entry 6). The yield as well as TON was decreased significantly when CuO powder having particle sizes in micron was employed as a catalyst for the reaction (Table 1, entry 7). A blank test, in absence of any catalyst, did not produce the desired product FDMC even after 20 h of the reaction (Table 1, entry 8). This indicates the slow kinetics of oxidative methyl-esterification reaction in the absence of the catalyst. Next, the reaction was tried to carry out using other oxidants such as molecular oxygen or hydrogen peroxide, but there was no formation of FDMC was observed in either cases (Table 1, entries 9 and 10). Next, the quantity of TBHP was optimized and it was found that the 8 mol% of TBHP provides the maximum yield of FDMC (Table 1, entries 11 and 12). Effect of solvents on the progress of the reaction was also studied. The lower yield of FDMC (68%) was obtained when the reaction was carried out in DMSO as the solvent (Table 1, entry 13). Similarly, water as well as methanol also provided the poor yield of FDMC 63% and 44% respectively (Table 1, entries 14 and 15). The maximum yield of the FDMC was obtained when the mixture of DMSO (3 mL) and water (1 mL) was used as the solvent.

Table 1 Optimization of the reaction conditions for oxidative methyl-esterification of HMF.^[a]

							
Entry	Catalyst	Temperature [°C]	Oxidant	TON	Conversion n ^[b] [%]	Yields ^[b] [%]	
						FDMC	FMF
1	CuO/N-C-HNSs	80	TBHP	18.2	66	34	24
2	CuO/N-C-HNSs	90	TBHP	30.6	83	58	17
3	CuO/N-C-HNSs	100	TBHP	49.2	100	93	-
4	CuO/N-C-HNSs	110	TBHP	48.8	100	92	-
5	N-C-HNSs	100	TBHP	-	9	-	-
6 ^c	CuO	100	TBHP	1	84	56	15
7 ^d	CuO	100	TBHP	0.6	57	35	18

8	Blank	100	TBHP	-	8	-	-
9	CuO/N-C-HNSs	100	O ₂	-	6	-	-
10	CuO/N-C-HNSs	100	H ₂ O ₂	-	10	-	-
11 ^e	CuO/N-C-HNSs	100	TBHP	40.2	100	78	16
12 ^f	CuO/N-C-HNSs	100	TBHP	48.0	100	91	-
13 ^g	CuO/N-C-HNSs	100	TBHP	36.0	94	68	-
14 ^h	CuO/N-C-HNSs	100	TBHP	33.2	100	63	18
15 ⁱ	CuO/N-C-HNSs	100	TBHP	23.4	74	44	-

[a] Reaction conditions: HMF, 1 mmol; catalyst, 50 mg; TBHP, 8 mmol; solvent, DMSO: Water (3mL:1mL); time, 20 h. [b] Conversion and yields were determined by GC. [c] CuO bulk nanopowder <50 nm. [d] CuO bulk powder. [e] TBHP, 6 mmol. [f] TBHP, 10 mmol. [g] Solvent, DMSO (4 mL). [h] Solvent, water (4 mL). [i] Solvent, methanol (4 mL).

The effect of CuO/N-C-HNSs loading on one-pot conversion of HMF into FDMC was studied comprehensively and the outcomes are presented in Fig. 7a. Increasing the loading of CuO/N-C-HNSs from 1 to 2 mol% increased the yield of FDMC from 38% to 93% which could be possibly due to the more number of catalytic sites available for the reaction. However, further increment in the loading of CuO/N-C-HNSs up to 2.5 mol% did not increase the yield of FDMC. This suggests that the 2 mol% loading of CuO/N-C-HNSs provides a sufficient quantity of catalytic sites in the reaction to achieve the maximum yield of FDMC. Next, the progress of the reaction was monitored at different time intervals (Fig. 7b). Analysis of the reaction mixture after 10 h shows that the mixture contains 26% of 5-formyl-2-methyl furoate (FMF) and 38% of FDMC. The quantity of FMF in the reaction mixture decreases gradually as the reaction time increases, whereas the quantity of FDMC increases continuously. This indicates that FMF is the intermediate product formed in one-pot conversion of HMF into FDMC using TBHP.

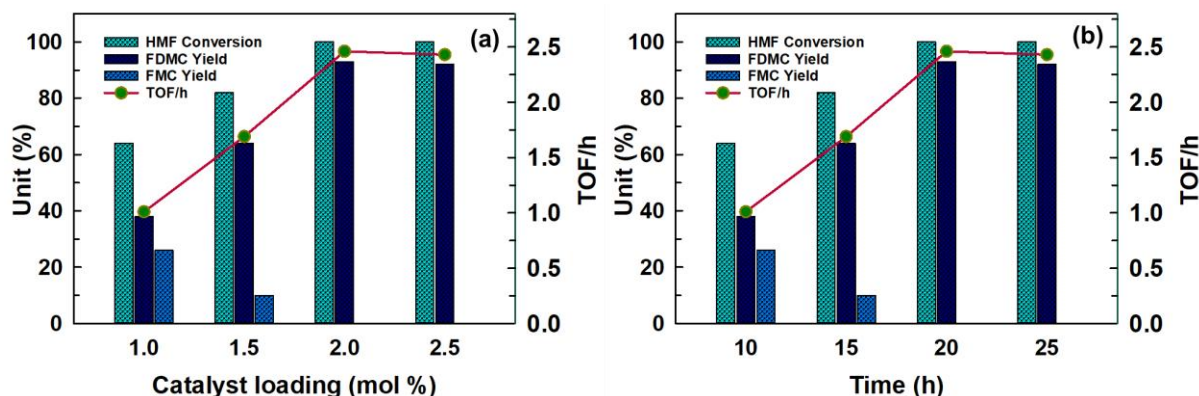
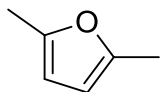
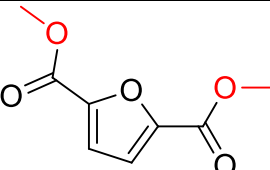
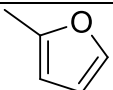
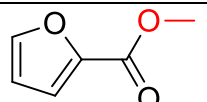
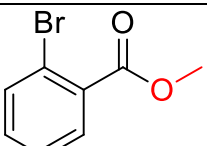
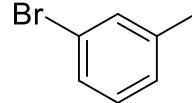
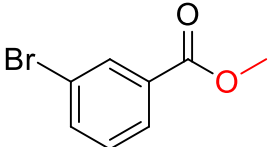
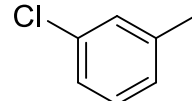
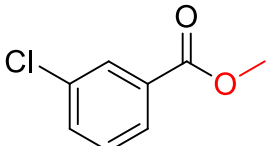
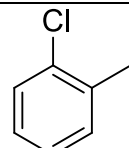
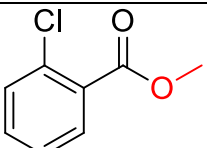


Fig. 7 Optimization study in oxidative methyl-esterification of HMF. (a) Effect of CuO/N-C-HNSs loading. Conditions: HMF, 1 mmol; CuO/N-C-HNSs, 1-2.5 mol%; TBHP, 8 mmol; DMSO:H₂O, 3mL:1mL; temperature, 100 °C; time, 20 h. (b) Effect of reaction time. Conditions: HMF, 1 mmol; CuO/N-C-HNSs, 2 mol%; TBHP, 8 mmol; DMSO: H₂O, 3mL: 1mL; temperature, 100 °C; time, 10-25 h.

2.2.2 Synthesis of different esters through *SP*³ C-H bond functionalization

To establish the wide applicability of CuO/N-C-HNSs in oxidative methyl-esterification reaction, a wide variety of substrates were efficiently converted in to the corresponding esters through functionalization of a less reactive *SP*³ C-H bond. As summarized in Table 2, various less reactive substrates were smoothly converted into the corresponding products in high yields through *SP*³ C-H bond functionalization.

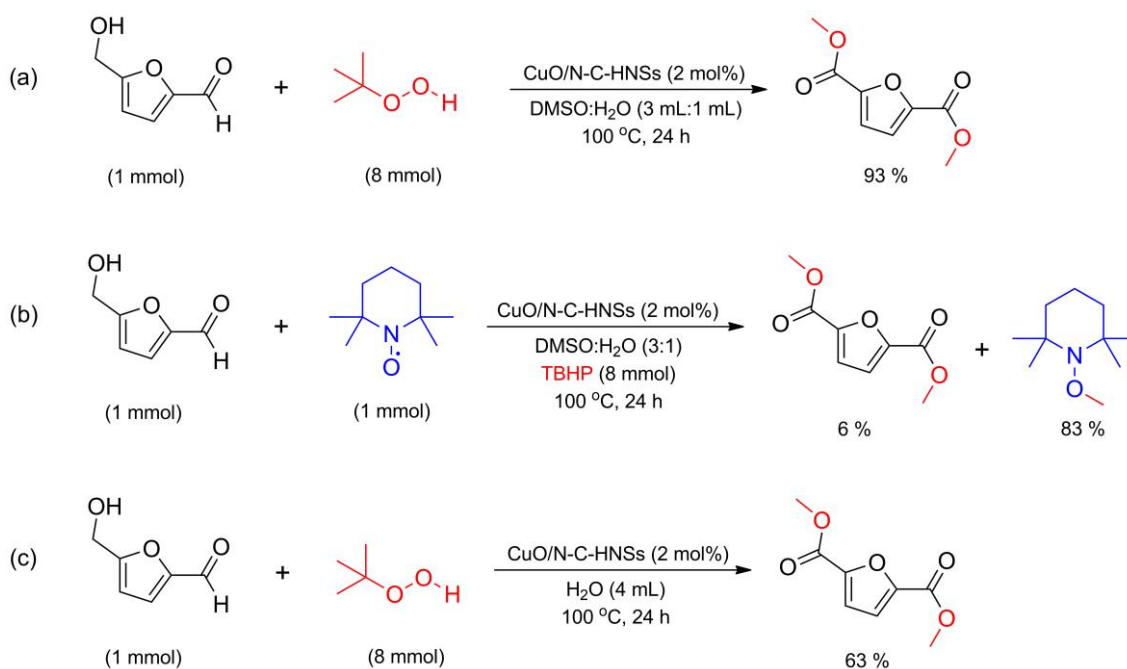
Table 2 Oxidative methyl-esterification via *SP*³ C-H bond functionalization.^[a]

Entry	Substrate	Product	Yield ^[b] (%)
1			73
2			76
3			86
4			88
5			87
6			83

[a] Reaction conditions: Substrate, 1 mmol; CuO/N-C-HNSs, 2 mol%; TBHP, 8 mmol; DMSO:H₂O, 3mL:1mL; temperature, 100 °C; time, 20 h. [b] GC yields.

2.3 Control experiments to study the reaction mechanism

A set of controlled experiments was performed to study the mechanism of the direct conversion of HMF into FDMC using TBHP and the outcomes are summarized in Scheme 1. When the reaction was carried out in presence of 1 equivalent of a radical scavenger, TEMPO (2,2,6,6-tetramethylpiperidine-*N*-oxyl) only 6% of the desired product was obtained where as 83% of 1-methoxy-2,2,6,6-tetramethylpiperidine was formed (Scheme 1b). This suggests that the reaction proceeds via a radical mechanism and involves the formation of methyl radicals in the catalytic cycle. Next, to identify the source of methyl radical whether it comes from the TBHP or DMSO, the reaction was carried out using water as the only solvent, and the FDMC was obtained in 63% yield. Therefore, it is confirmed that the methyl radicals come from the TBHP (Scheme 1c). Thus, it can be concluded that the TBHP plays a dual role as it acts as the oxidizing agent as well as the methylating reagent in oxidative methyl-esterification of HMF.

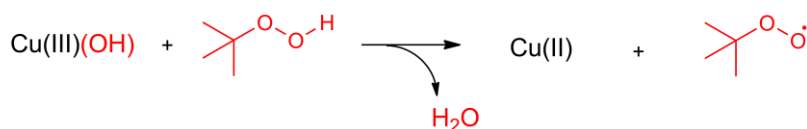


Scheme 1 Control experiments and the effect of radical scavenger.

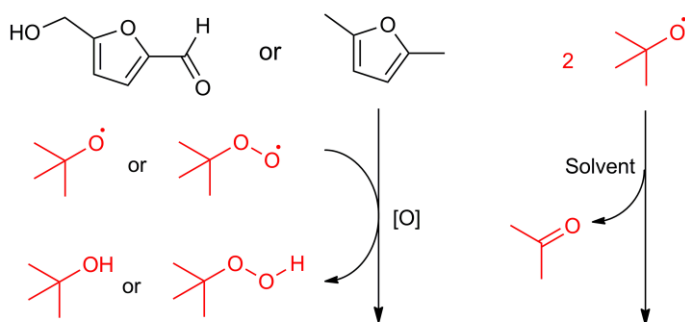
Taking into consideration the outcome of control experimentations and previous reports [51,53,60], a plausible mechanism is presented (Scheme 2). The reaction begins with generation of a *tert*-butoxyl or *tert*-butylperoxyl radicals from TBHP in the presence of CuO/N-C-HNSs (Step I, Scheme 2). Next, *tert*-butoxyl radical undergoes a unimolecular decomposition generating acetone and a methyl radical. The starting material, HMF or 2,5-dimethylfuran in presence of TBHP and catalyst undergoes oxidation affording the formation of acyloxyl

radical. In the last step, acyloxyl radical reacts with methyl radicals and generates the desired product (Step III, Scheme 2).

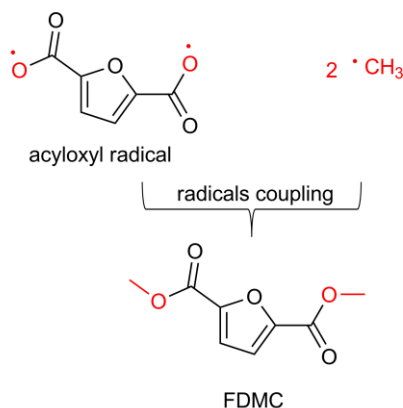
Step I :



Step II :



Step III :



Scheme 2 Plausible mechanism for oxidative methyl-esterification of HMF using TBHP.

2.4 Catalyst stability and recyclability

The recyclability of CuO/N-C-HNSs was also investigated. During the recycling study, the CuO/N-C-HNSs was isolated by centrifugation and then washed with a mixture of water and ethanol. The washed catalyst was dried at 100 °C for 12 h and then used for the next batch of reaction. The result shows a marginal decrease in the yield of FDMC from 93% to 81% and the TOF from 2.46 h⁻¹ to 2.14 h⁻¹ during the recycling of CuO/N-C-HNSs for 4 times (Figure 8). The hot-filtration test was carried out to confirm the heterogeneity of CuO/N-C-HNSs in oxidative methyl-esterification reaction. During hot-filtration test, the reaction was stopped after 5h, and the catalyst was removed from the reaction mixture by filtration, and then the reaction was further continued for 15h using the filtrate. The conversion, as well as yield,

remained constant after the removal of catalyst from the reaction mixture indicating the heterogeneous nature of CuO/N-C-HNSs. The SEM, TEM and HRTEM images of CuO/N-C-HNSs after recycling for 4 times were recorded. The SEM images (Figure S4, ESI) show the retention of original structure and morphology in the recycled CuO/N-C-HNSs. TEM and HRTEM images (Figure S5 and S6, ESI) reveal the absence of agglomeration of CuO nanoparticles on the surface of N-C-HNSs in the recycled catalyst. The powder XRD of CuO/N-C-HNSs recycled for 4 times (Figure S7, ESI) shows the diffraction pattern similar to the fresh catalyst suggesting no structural changes in the recycled catalyst. Thus, the various characterizations of the recycled catalyst confirm the high stability of the CuO/N-C-HNSs in the oxidative methyl-esterification of HMF.

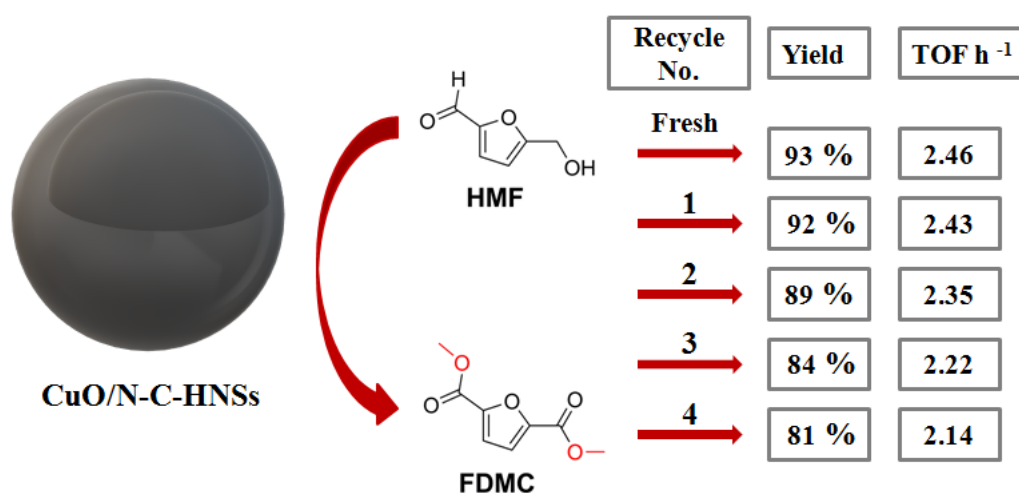


Fig. 8 Recyclability of CuO/N-C-HNSs in oxidative methyl-esterification of HMF.

3. Conclusions

In conclusion, we have demonstrated a one-pot synthesis of FDMC from HMF in the presence of TBHP using a novel material, ultrafine CuO particles dispersed on nitrogen-doped carbon hollow nanospheres (CuO/N-C-HNSs) as a catalyst. N-doping provided a strong interaction between the support and metal affording ultrafine dispersion of CuO nanoparticles on the surface of N-C-HNSs and also prevented the agglomeration of CuO nanoparticles during the catalyst recycling. The hollow spherical structure resulting from the removal of SiO₂ facilitates the mass transfer of reactants and products thereby regenerating the catalytic sites for further reactions. The mechanistic study reveals that the reaction proceeds through formation and coupling of radical intermediates and TBHP plays a dual role, it acts as an oxidizing as well as methylating reagent. In addition to HMF, a wide variety of substrates were also converted into the corresponding esters through functionalization of a

less reactive SP^3 C-H bond establishing the broad applicability of the CuO/N-C-HNSs in oxidative methyl-esterification reaction.

4. Experimental details

4.1 Synthesis of CuO/N-C-HNSs

For the synthesis of CuO/N-C-HNSs, first SiO_2 nanospheres with particle sizes between 100-150 nm was prepared by a modified Stöber's method.^[61] In a typical procedure, 3 mL of TEOS was added into a beaker containing 100 mL of ethanol under continuous stirring. To the resulting mixture, 6 mL of ammonia and 6 mL of distilled water was added and the reaction mixture was kept stirring for 5 h at room temperature. The colourless solution gradually turned into a turbid suspension indicating the formation of colloidal SiO_2 nanoparticles. The SiO_2 nanoparticles were isolated by centrifugation at 10000 rpm for 10 min and then washed with distilled water and ethanol mixture several times by centrifugation and redispersion. The obtained solid was dried at 80 °C for 12 h and then grinds to obtain SiO_2 nanospheres.

Next, the surface of the as-prepared SiO_2 nanospheres was functionalized with negative charges using poly(diallyldimethylammonium chloride) solution (PDDA) and poly(sodium 4-styrenesulfonate) solution (PSS) polymers.^[49] Specifically, the as-prepared SiO_2 nanospheres (0.6 g) were dispersed in 100 mL distilled water containing 3 g NaCl by ultra sonication for 30 min. To the resulting suspension, 1 g of PDDA solution was added, and the mixture was kept stirring for 1 h at room temperature. After that, the PDDA-modified SiO_2 nanospheres were isolated and washed with distilled water by centrifugation at 10000 rpm for 10 min. Following the similar procedure, the surface of the PDDA-modified SiO_2 nanospheres was further coated with the layers of PSS, PDDA and PSS successively to obtain the negatively charged PDDA/PSS/PDDA/PSS-modified SiO_2 nanospheres. Subsequently, 500 mg of the PDDA/PSS/PDDA/PSS-modified SiO_2 nanospheres were dispersed by ultra sonication in 10 mL distilled water containing 50 mg of copper (II) nitrate trihydrate. To the above suspension, 200 mg of histidine was added and kept stirring for 30 min at room temperature. The resulting mixture was vacuum-dried at 80 °C for 2h and then pyrolyzed in N_2 atmosphere at 800 °C for 3h with a heating rate of 2 °C min^{-1} . The SiO_2 template in the pyrolyzed product was removed by etching with 2M NaOH (50 mL) for 24h at room temperature and then washed with distilled water several times and dried for overnight at 100 °C to obtain the final product CuO/N-C-HNSs.

4.2 Process for the oxidative methyl-esterification reaction

All the oxidative methyl-esterification reactions were carried out in an oven-dried glass vial. In a typical procedure, the glass vial was charged with substrate (1 mmol), 70% aqueous TBHP (1 mL), catalyst (20 mg) and solvent dimethyl sulfoxide (DMSO): water (3:1) 4 mL. The glass vial was sealed with an aluminium cap fitted with a Teflon coated rubber septum and the reaction mixture was heated in an oil bath at 100 °C for 20 h under continuous stirring. After 20 h, the reaction mixture was allowed to cool at room temperature and then subjected to centrifugation for 10 min at 10000 rpm. After centrifugation, the catalyst get settled at the bottom of the centrifuge tube and the clear supernatant liquid was transferred into a separating funnel containing 100 mL of water and mixed thoroughly. Ethyl acetate (40 mL x 2 times) was used as a solvent for extraction of the organic components from the aqueous mixture. The dried organic portion was evaporated under vacuum to obtain the crude product which was later purified by column chromatography and finally characterized by GC-MS and NMR spectroscopy.

Acknowledgements:

Author MLK sincerely acknowledge Science and Engineering Research Board, Department of Science and Technology, India for providing J.C. Bose national fellowship. Authors are greatly thankful to the Godrej Industries Limited, India for providing financial support.

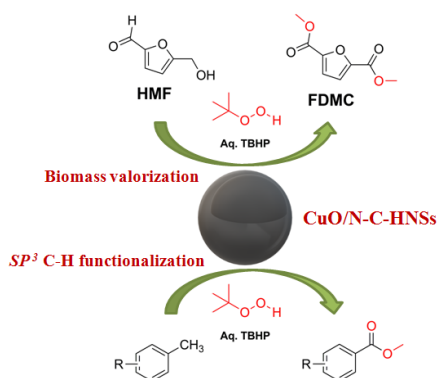
References:

- [1] Y. Zhu, C. Romain, C. K. Williams, *Nature* **2016**, *540*, 354–362.
- [2] R. A. Sheldon, *Green Chem.* **2014**, *16*, 950–963.
- [3] S. S. R. Gupta, M. L. Kantam, *Catal. Today* **2018**, *309*, 189–194.
- [4] S. S. R. Gupta, M. L. Kantam, *Catal. Commun.* **2019**, *124*, 62–66.
- [5] H. Xia, J. An, M. Hong, S. Xu, L. Zhang, S. Zuo, *Catal. Today* **2019**, *319*, 113–120.
- [6] J. An, G. Sun, H. Xia, *ACS Sustain. Chem. Eng.* **2019**, *7*, 6696–6706.
- [7] M. Hong, S. Wu, J. Li, J. Wang, L. Wei, K. Li, *Catal. Commun.* **2020**, *136*, 105909.
- [8] S. Mhadmhan, A. Franco, A. Pineda, P. Reubroycharoen, R. Luque, *ACS Sustain. Chem. Eng.* **2019**, *7*, 14210–14216.
- [9] R.-J. van Putten, J. C. van der Waal, E. de Jong, C. B. Rasrendra, H. J. Heeres, J. G. de Vries, *Chem. Rev.* **2013**, *113*, 1499–1597.
- [10] M. A. Hillmyer, *Science*. **2017**, *358*, 868–870.

- [11] X. Huang, J. Song, M. Hua, Z. Xie, S. Liu, T. Wu, G. Yang, B. Han, *Green Chem.* **2020**, *22*, 843–849.
- [12] X. Liao, J. Hou, Y. Wang, H. Zhang, Y. Sun, X. Li, S. Tang, K. Kato, M. Yamauchi, Z. Jiang, *Green Chem.* **2019**, *21*, 4194–4203.
- [13] S. Xu, P. Zhou, Z. Zhang, C. Yang, B. Zhang, K. Deng, S. Bottle, H. Zhu, *J. Am. Chem. Soc.* **2017**, *139*, 14775–14782.
- [14] A. Tirsoaga, M. El Fergani, N. Nuns, P. Simon, P. Granger, V. I. Parvulescu, S. M. Coman, *Appl. Catal. B Environ.* **2020**, *278*, 119309.
- [15] T. Gao, Y. Yin, G. Zhu, Q. Cao, W. Fang, *Catal. Today* **2020**, *355*, 252–262.
- [16] H. Xia, J. An, W. Zhang, *Nanomaterials* **2020**, *10*, 1624.
- [17] A. F. Sousa, C. Vilela, A. C. Fonseca, M. Matos, C. S. R. Freire, G.-J. M. Gruter, J. F. J. Coelho, A. J. D. Silvestre, *Polym. Chem.* **2015**, *6*, 5961–5983.
- [18] J. Zhu, J. Cai, W. Xie, P.-H. Chen, M. Gazzano, M. Scandola, R. A. Gross, *Macromolecules* **2013**, *46*, 796–804.
- [19] S. K. Burgess, J. E. Leisen, B. E. Kraftschik, C. R. Mubarak, R. M. Kriegel, W. J. Koros, *Macromolecules* **2014**, *47*, 1383–1391.
- [20] S. Weinberger, K. Haernvall, D. Scaini, G. Ghazaryan, M. T. Zumstein, M. Sander, A. Pellis, G. M. Guebitz, *Green Chem.* **2017**, *19*, 5381–5384.
- [21] X. Kong, Y. Zhu, Z. Fang, J. A. Kozinski, I. S. Butler, L. Xu, H. Song, X. Wei, *Green Chem.* **2018**, *20*, 3657–3682.
- [22] G. Yi, S. P. Teong, Y. Zhang, *Green Chem.* **2016**, *18*, 979–983.
- [23] A. J. J. E. Eerhart, A. P. C. Faaij, M. K. Patel, *Energy Environ. Sci.* **2012**, *5*, 6407.
- [24] C. F. Araujo, M. M. Nolasco, P. J. A. Ribeiro-Claro, S. Rudić, A. J. D. Silvestre, P. D. Vaz, A. F. Sousa, *Macromolecules* **2018**, *51*, 3515–3526.
- [25] E. Taarning, I. S. Nielsen, K. Egeblad, R. Madsen, C. H. Christensen, *ChemSusChem* **2008**, *1*, 75–78.
- [26] O. Casanova, S. Iborra, A. Corma, *J. Catal.* **2009**, *265*, 109–116.
- [27] M. Kim, Y. Su, T. Aoshima, A. Fukuoka, E. J. M. Hensen, K. Nakajima, *ACS Catal.* **2019**, *9*, 4277–4285.
- [28] J. Du, H. Fang, H. Qu, J. Zhang, X. Duan, Y. Yuan, *Appl. Catal. A Gen.* **2018**, *567*, 80–89.
- [29] D. K. Mishra, J. K. Cho, Y. Yi, H. J. Lee, Y. J. Kim, *J. Ind. Eng. Chem.* **2019**, *70*, 338–345.
- [30] A. Buonerba, S. Impemba, A. D. Litta, C. Capacchione, S. Milione, A. Grassi,

- ChemSusChem* **2018**, *11*, 3139–3149.
- [31] A. Cho, S. Byun, J. H. Cho, B. M. Kim, *ChemSusChem* **2019**, *12*, 2310–2317.
- [32] F. Menegazzo, M. Signoretto, D. Marchese, F. Pinna, M. Manzoli, *J. Catal.* **2015**, *326*, 1–8.
- [33] J. Deng, H.-J. Song, M.-S. Cui, Y.-P. Du, Y. Fu, *ChemSusChem* **2014**, *7*, 3334–3340.
- [34] Y. Sun, H. Ma, X. Jia, J. Ma, Y. Luo, J. Gao, J. Xu, *ChemCatChem* **2016**, *8*, 2907–2911.
- [35] K. Sun, S. Chen, Z. Li, G. Lu, C. Cai, *Green Chem.* **2019**, *21*, 1602–1608.
- [36] H. Zhou, S. Hong, H. Zhang, Y. Chen, H. Xu, X. Wang, Z. Jiang, S. Chen, Y. Liu, *Appl. Catal. B Environ.* **2019**, *256*, 117767.
- [37] A. Salazar, P. Hünemörder, J. Rabeah, A. Quade, R. V. Jagadeesh, E. Mejia, *ACS Sustain. Chem. Eng.* **2019**, *7*, 12061–12068.
- [38] K. S. Kozlov, L. V. Romashov, V. P. Ananikov, *Green Chem.* **2019**, *21*, 3464–3468.
- [39] F. Li, X.-L. Li, C. Li, J. Shi, Y. Fu, *Green Chem.* **2018**, *20*, 3050–3058.
- [40] Y. Feng, W. Jia, G. Yan, X. Zeng, J. Sperry, B. Xu, Y. Sun, X. Tang, T. Lei, L. Lin, *J. Catal.* **2020**, *381*, 570–578.
- [41] A. Salazar, A. Linke, R. Eckelt, A. Quade, U. Kragl, E. Mejía, *ChemCatChem* **2020**, *12*, 3504–3511.
- [42] T. Rui, G.-P. Lu, X. Zhao, X. Cao, Z. Chen, *Chinese Chem. Lett.* **2020**, DOI 10.1016/j.cclet.2020.06.027.
- [43] Y. Lin, G.-P. Lu, X. Zhao, X. Cao, L. Yang, B. Zhou, Q. Zhong, Z. Chen, *Mol. Catal.* **2020**, *482*, 110695.
- [44] T. Ghosh, P. Chandra, A. Mohammad, S. M. Mobin, *Appl. Catal. B Environ.* **2018**, *226*, 278–288.
- [45] S. S. R. Gupta, A. Vinu, M. L. Kantam, *J. Catal.* **2020**, *389*, 259–269.
- [46] W. Gong, Y. Lin, C. Chen, M. Al-Mamun, H. Lu, G. Wang, H. Zhang, H. Zhao, *Adv. Mater.* **2019**, *31*, 1808341.
- [47] X. Han, X. Ling, Y. Wang, T. Ma, C. Zhong, W. Hu, Y. Deng, *Angew. Chemie Int. Ed.* **2019**, *58*, 5359–5364.
- [48] D. A. Bulushev, A. L. Chuvilin, V. I. Sobolev, S. G. Stolyarova, Y. V. Shubin, I. P. Asanov, A. V. Ishchenko, G. Magnani, M. Riccò, A. V. Okotrub, L. G. Bulusheva, *J. Mater. Chem. A* **2017**, *5*, 10574–10583.
- [49] Y. Chen, Z. Li, Y. Zhu, D. Sun, X. Liu, L. Xu, Y. Tang, *Adv. Mater.* **2019**, *31*, 1806312.

- [50] W. Stöber, A. Fink, E. Bohn, *J. Colloid Interface Sci.* **1968**, *26*, 62–69.
- [51] S. Wang, Z. Zhang, B. Liu, *ACS Sustain. Chem. Eng.* **2015**, *3*, 406–412.
- [52] F. A. Kucherov, L. V. Romashov, K. I. Galkin, V. P. Ananikov, *ACS Sustain. Chem. Eng.* **2018**, *6*, 8064–8092.
- [53] Y. Zhu, H. Yan, L. Lu, D. Liu, G. Rong, J. Mao, *J. Org. Chem.* **2013**, *78*, 9898–9905.
- [54] P. S. Samudrala, A. V. Nakhate, S. S. R. Gupta, K. B. Rasal, G. P. Deshmukh, C. R. Gadipelly, S. Theegala, D. K. Dumbre, S. Periasamy, V. R. C. Komandur, S. K. Bhargava, L. K. Mannepalli, *Appl. Catal. B Environ.* **2019**, *240*, 348-357.
- [55] S. S. R. Gupta, A. V. Nakhate, K. B. Rasal, G. P. Deshmukh, L. K. Mannepalli, *New J. Chem.* **2017**, *41*, 15268-15276.
- [56] S. S. R. Gupta, A. V. Nakhate, G. P. Deshmukh, S. Periasamy, P. S. Samudrala, S. K. Bhargava, M. Lakshmi Kantam, *ChemistrySelect* **2018**, *3*, 8436-8443.
- [57] C. Tang, Y. Liu, C. Xu, J. Zhu, X. Wei, L. Zhou, L. He, W. Yang, L. Mai, *Adv. Funct. Mater.* **2018**, *28*, 1704561.
- [58] W. Li, C. Min, F. Tan, Z. Li, B. Zhang, R. Si, M. Xu, W. Liu, L. Zhou, Q. Wei, Y. Zhang, X. Yang, *ACS Nano* **2019**, *13*, 3177–3187.
- [59] P. Jiang, D. Prendergast, F. Borondics, S. Porsgaard, L. Giovanetti, E. Pach, J. Newberg, H. Bluhm, F. Besenbacher, M. Salmeron, *J. Chem. Phys.* **2013**, *138*, 024704.
- [60] N. Khatun, S. K. Santra, A. Banerjee, B. K. Patel, *European J. Org. Chem.* **2015**, *2015*, 1309–1313.
- [61] X. Qiu, T. Li, S. Deng, K. Cen, L. Xu, Y. Tang, *Chem. - A Eur. J.* **2018**, *24*, 1246–1252.

Table of Contents:

One-pot synthesis of FDMC from oxidative methyl-esterification of HMF has been reported using a novel nanocomposite, CuO/N-C-HNSs as a catalyst and TBHP as an oxidizing and methylating reagent. The nitrogen-doped carbon nanospheres firmly anchored CuO and stabilized them in the form of clusters of less than 10 nm in size. In addition to HMF, the oxidative esterification involving SP^3 C-H bond functionalization has also been demonstrated using the same catalyst.